Proceedings of the 21st ICSMGE, Vienna, Austria, 14 – 19 June 2026. Pistrol, Adam & Schweiger (eds.)
Published by: ÖGG, Austrian Society for Geomechanics, Salzburg, Austria, ISBN 978-3-9503898-4-5
https://doi.org/10.53243/ICSMGE2026-352

Unveiling Complex Rock Mass Behavior: A Novel Approach Combining LiDAR Data and Numerical Simulation for Slope Design

Özgen Kökten
Temelsu International Engineering Services Inc., Türkiye, ozgen.kokten@temelsu.com.tr

Seray Zedeli
Temelsu International Engineering Services Inc., Türkiye, seray.sezgin@temelsu.com.tr

ABSTRACT: Accurate identification of critical and high-risk zones is essential for assessing rock slope stability, particularly in geologically complex regions where slope failure can severely impact vital infrastructure and environmental sustainability. This study investigates a significant large scale rock slope failure that occurred on the left abutment of a roller compacted concrete (RCC) gravity dam, situated within a region of strategic importance for energy production. Following the failure event, a comprehensive post failure analysis was conducted, involving detailed geostructural characterization of the rock mass. This included the mapping and analysis of joint networks, discontinuity orientations, and the spatial distribution of macro and micro scale fractures. High resolution terrestrial LiDAR scanning technology was employed to acquire dense and accurate point cloud datasets, enabling the generation of precise three dimensional mesh models of the slope surface. These models provided a reliable geometric basis for subsequent mechanical analyses. To realistically simulate the complex stress-strain response of the fractured rock mass, advanced numerical models were developed, incorporating both conventional and elastoplastic constitutive frameworks. These models were calibrated meticulously using site specific geological and geomechanical data to reflect the anisotropic behavior dictated by the discontinuity systems. In parallel, probabilistic rockfall simulations were performed using stochastic seeding approaches to predict potential trajectories, bounce heights, and final resting locations of mobilized rock blocks under variable initial conditions. The integration of LiDAR derived high resolution point clouds with advanced numerical modeling significantly improved the accuracy and reliability of slope failure analyses. Within the scope of this study, failure mechanisms observed in the field were effectively replicated by high fidelity numerical simulations based on detailed LiDAR geometry and discontinuity mapping, resulting in a strong correlation between modeled behavior and the actual failure pattern. This integrated methodology demonstrates substantial potential for enhancing hazard assessment in critical engineering environments.

KEYWORDS: Rock slope stability, roller compacted concrete (RCC) dam, LiDAR scanning, numerical modeling, rockfall simulation

1 INTRODUCTION

Rock slope stability remains a pivotal challenge within geotechnical engineering, particularly when situated in geologically heterogeneous terrains underpinning critical infrastructure such as dams, highways, and energy facilities. The inherent discontinuous nature of rock masses manifested through joints, faults, and fractures significantly governs slope behavior and failure mechanisms. Accurate characterization of these structural discontinuities is essential for reliable assessment and mitigation of rock slope failures, which can have profound environmental consequences.

Roller compacted concrete (RCC) gravity dams have gained prominence due to their expedited construction timelines and cost-effectiveness. However, the geological complexity of their abutment slopes often poses significant stability challenges that necessitate rigorous investigation. Within the scope of this study, a prominent RCC gravity dam is examined as a detailed case study to elucidate the interplay between geological discontinuities and stress redistribution patterns influencing slope failure. The general layout of the dam site, along with the visual representation of the observed slope failure, is illustrated in Figures 1 and 2, respectively. This targeted analysis enables a nuanced understanding of failure mechanisms specific to RCC dam environments, where conventional survey techniques frequently fall short in capturing the detailed geometry and spatial variability of discontinuity networks. Consequently, enhancing the resolution and accuracy of structural characterization is imperative for developing robust predictive models tailored to such critical infrastructure.

Advancements in remote sensing technologies, notably terrestrial LiDAR, have revolutionized the acquisition of high-resolution spatial data, enabling detailed three dimensional reconstruction of slope surfaces and discontinuity mapping. When integrated with sophisticated numerical modeling frameworks that incorporate anisotropic and elasto-plastic constitutive behaviors, these datasets provide unprecedented insights into rock mass response under varying loading scenarios.

Moreover, probabilistic rockfall simulations informed by stochastic seeding enhance the understanding of kinematic behaviors of mobilized rock blocks, facilitating risk quantification and hazard mitigation strategies. This study leverages such integrated methodologies to investigate a significant rock slope failure adjacent to an RCC dam, aiming to bridge the gap between field observations and numerical predictions. The outcomes contribute to the refinement of slope stability analysis techniques applicable to critical infrastructure situated in complex geological contexts.

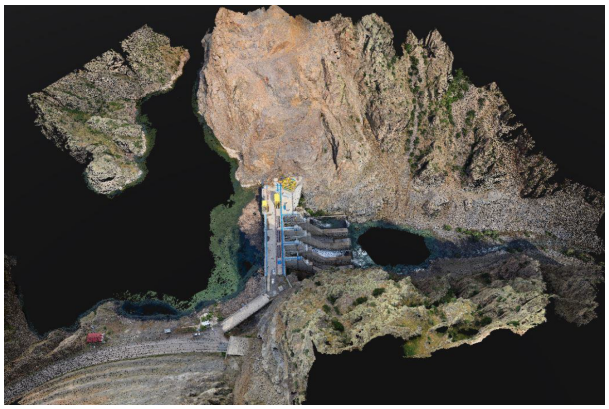

Figure 1. General overview of the dam site

Figure 2. General view of the rock slope failure

2 GEOLOGICAL CONDITION

2.1 *Regional stratigraphy*

The volcanic and plutonic rock assemblages observed within the project site and its immediate surroundings are interpreted as products of subduction-related magmatic processes developed in the context of convergent plate tectonic regimes. These rocks likely originated during the subduction of oceanic lithosphere beneath a continental margin, resulting in the formation of a typical magmatic arc environment. In contrast, the Neogene-aged sedimentary units in the region were deposited in continental settings during post-collisional phases that followed the closure of oceanic basins, representing a later stage in the tectonic evolution of the area.

Within the project area and approximately 1.5 km both upstream and downstream along the valley, the lithological assemblage is characterized by the exposure of the Ikizdere Magmatics. These outcrops exhibit highly irregular geometries, suggesting that they represent marginal zones or apophyses of a larger intrusive body, most plausibly associated with the Rize Pluton. Field investigations and petrographic analyses of representative samples reveal that the Ikizdere Magmatics are composed primarily of granitic and granitoid rocks, including granodiorite-tonalite, adamellite, porphyritic microgranite, and granite-gneiss. Thin-section examinations further indicate that these main units are locally intruded by andesitic dykes and are spatially associated with a variety of additional intrusive lithologies such as mangerite, pyroxene-bearing mangerite, granite porphyry, granogabbro, and alkaline granite.

These observations suggest that the exposed magmatic rocks do not constitute isolated lithological bodies but instead represent differentiated segments of a vertically and laterally evolved magmatic system. When considered together, the mineralogical and textural characteristics of the granodiorite-tonalite, adamellite, porphyritic microgranite, and granite-gneiss units display systematic compositional trends and volumetric variations in constituent minerals. These features support the interpretation that the various lithologies correspond to different facies or structural domains within a single, genetically related granitic intrusion.

Both macroscopic observations in the field and petrographic analyses indicate that the granitic rocks exhibit a range of textures, including aphanitic, porphyritic, and granophyric fabrics. Notably, there is no evidence of pronounced foliation or well-developed flow structures, suggesting that crystallization occurred under relatively static conditions with minimal influence from tectonic deformation or syn-magmatic shearing.

2.2 *Field and laboratory test results*

The mechanical behavior of the granitic rock mass was rigorously characterized through a combination of in-situ hydraulic jack tests and laboratory evaluations of core specimens. Field tests were performed in investigation galleries along the dam abutments in accordance with ASTM D1196, providing reliable measurements of deformation under actual stress conditions. Complementary laboratory testing included uniaxial and triaxial compressive strength assessments (ASTM D7012) and elastic modulus determination (ASTM D4543).

Laboratory specimens were subjected to stepwise hydraulic jack loading following ISRM Suggested Methods (2007), with an initial pre-load of 2–5 % of the estimated uniaxial compressive strength to ensure seating, followed by incremental load steps of 10–25 % of the estimated strength, each maintained until axial deformation stabilized. In the field, hydraulic jack loads typically ranged between 2 and 8 MPa per step, reflecting common practice for high strength granitic rock. This approach captured the nonlinear stress–strain response and peak strength, yielding reproducible mechanical parameters directly comparable to in-situ rock mass behavior.

The resulting deformation modulus (E_{def}) and secant elastic modulus (E_{sec}) from field tests are presented in Figure 3, while laboratory-derived intact rock strength and deformation characteristics are summarized in Table 1.

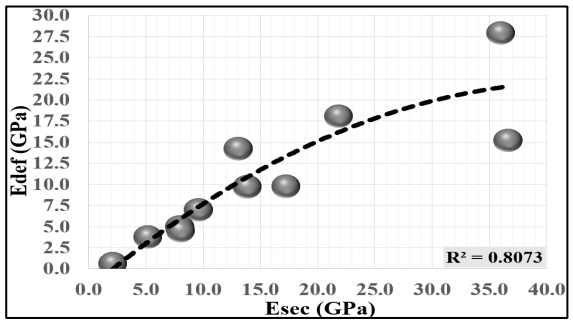

Figure 3. Field PLT rock deformation and secant modulus

Table 1. Laboratory test results.

Parameter	Symbol	Value	Unit
Median Intact Young's modulus	*E*	62.8	GPa
Median Uniaxial Compressive Strength	*UCS*	102.4	MN/m^2
Median Natural Unit Weight	γ	26.2	kN/m^3
Median Cohesion	c	40.0	kN/m^2
Median Internal Friction Angle	ϕ	48.5	o
Poisson's ratio	v	0.22	-

2.3 *Rock mass classification*

An integrated geomechanical characterization of the granitic rock masses exposed within the project site was performed utilizing both the Rock Mass Rating (RMR89) system and the Geological Strength Index (GSI), in accordance with the guidelines proposed by Hoek and Brown (1997, 2002). The classification approach incorporated lithological features, joint surface conditions, spacing, persistence, groundwater influence, and degree of weathering. As a result of this

comprehensive assessment, the GSI value for the intact to moderately jointed granite was estimated to be 70, reflecting a good quality rock mass. The evaluated GSI classification is presented in Figure 4.

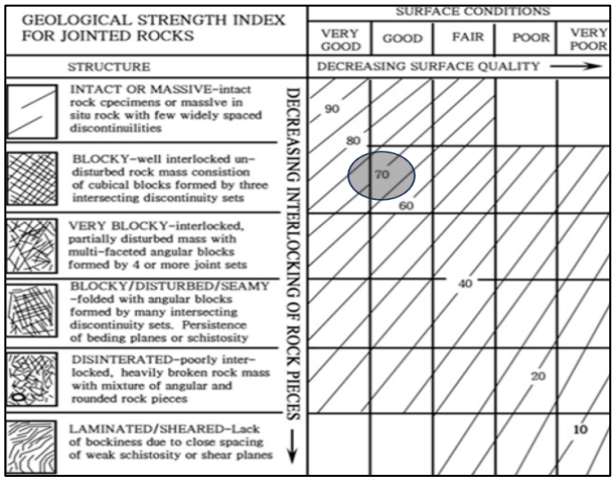

Figure 4. The evaluated GSI classification

2.4 *Rock slope joint set orientations*

Figures 5. Stereographic pole representations of the joint set orientations that control slope stability, identified through detailed field observations and high-resolution LiDAR imaging of the rock slope. The color coding in the figures indicates structural zones evaluated within the slope: green represents the hardway, red the grain, and yellow the rift directions.

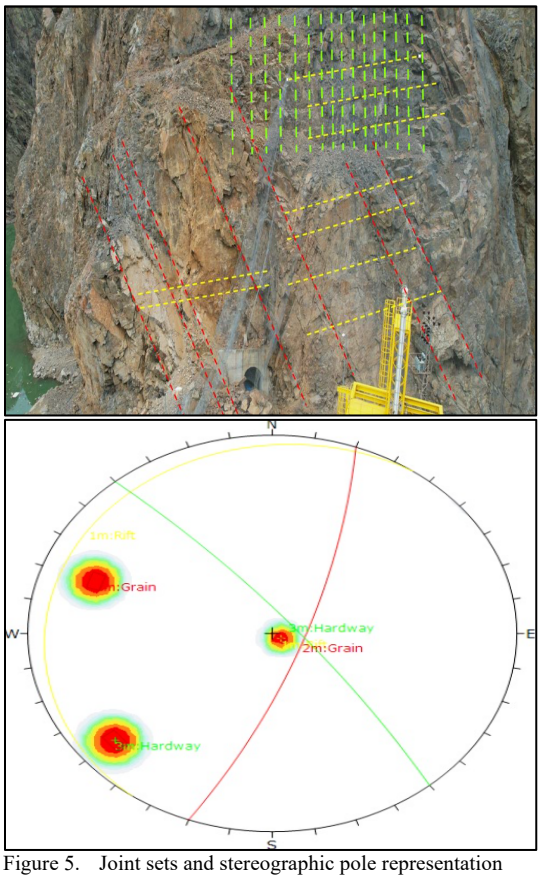

Figure 5. Joint sets and stereographic pole representation

3 HIGH RESOLUTION LIDAR BASED STRUCTURAL CHARACTERIZATION OF THE ROCK SLOPE

In order to precisely assess the existing condition of the left abutment rock slope of the RCC dam, define the geometrical and structural features of critical sections to be analyzed numerically, and to spatially determine and delineate the zones where stabilization measures are to be applied, high-resolution digital surface models were generated through the integration of photogrammetry and LiDAR (Light Detection and Ranging) technologies.

Within the scope of the photogrammetric campaign, a series of aerial images were acquired using a calibrated metric camera mounted on an unmanned aerial vehicle. The images were processed using PIX4Dmapper software, and georeferenced with ground control points to ensure high spatial accuracy. As a result, an orthorectified mosaic, dense point cloud data, and a 3D textured mesh model of the slope were produced.

In parallel, terrestrial LiDAR scanning was employed to capture high-density spatial data by recording laser pulses reflected from the terrain. These datasets were post-processed in Atlascan software to generate detailed and georeferenced point clouds.

The point clouds derived from both photogrammetric and LiDAR sources were subsequently merged using PIX4DSurvey software to construct a comprehensive and high-fidelity spatial model. This unified dataset facilitated the vectorization of key slope features, including overall geometry, visible discontinuity sets, minor and major joint traces, fragmented rock masses, inspection gallery structures, and critical surface elements located along the dam crest.

The resulting geospatial database provided essential input parameters for advanced numerical modeling and was instrumental in visualizing the structural behavior of the slope. These outputs, representing the spatial context and failure characteristics of the left abutment, are illustrated in Figures 6 through 9.

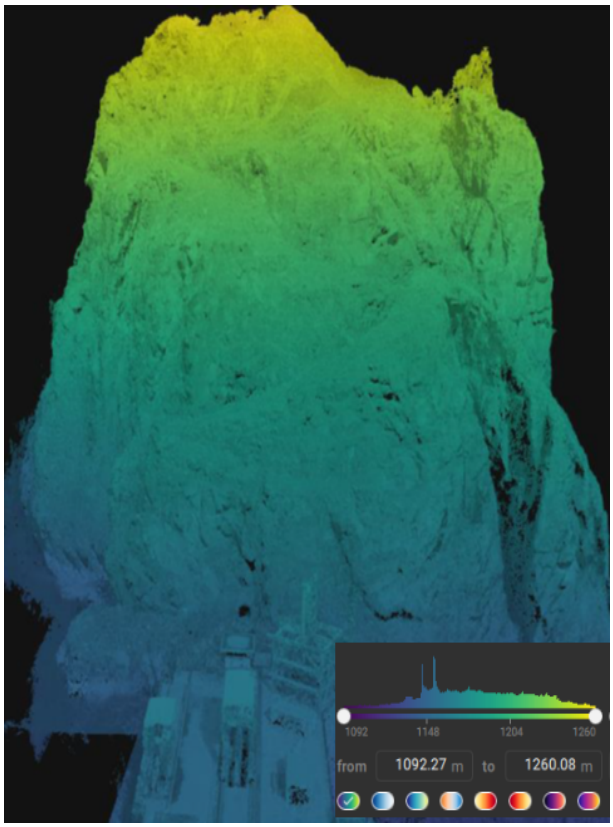

Figure 6. Elevation variation map of the rock slope

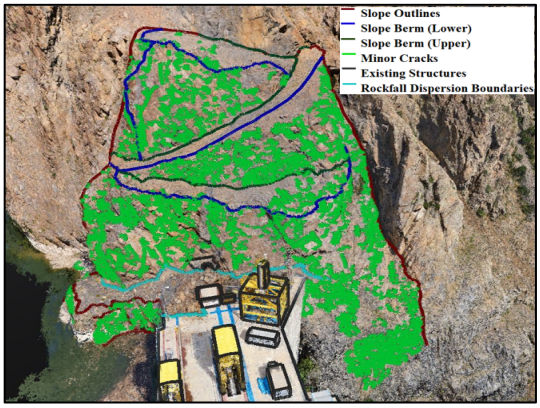

Figure 7. Characterized minor cracks

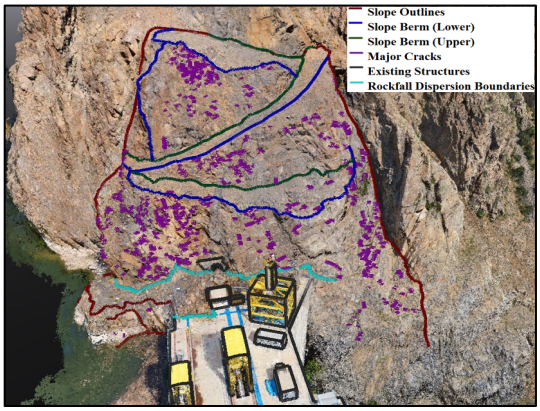

Figure 8. Characterized major cracks

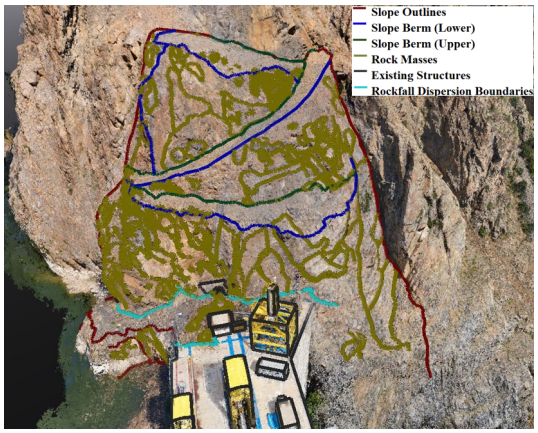

Figure 9. Characterized rock blocks

4 NUMERICAL ANALYSES

As part of the integrated slope failure assessment, high resolution LiDAR data combined with comprehensive geotechnical investigations were employed to accurately identify the most critical section of the failed rock slope. These datasets provided a detailed representation of the slope's morphology and structural characteristics, which formed the basis for subsequent numerical modeling. Utilizing the finite element software PLAXIS 2D v.2024.3, advanced stress deformation analyses were conducted to simulate the mechanical response of the rock mass under prevailing geological conditions and applied loads. In parallel, two-dimensional rockfall simulations were performed using the Rockfall V8.018 software package in order to evaluate the dynamic behavior of potential falling rock blocks along the slope face.

These simulations helped estimate the spatial extent of runout zones, bounce heights, and kinetic energy profiles associated with various seeder points. The general layout of the left abutment slope, encompassing major structural discontinuities and existing infrastructural elements, was meticulously examined to inform the selection of the modeling domain and boundary conditions. This comprehensive spatial framework, along with the critical area selected for detailed numerical evaluation, is depicted in Figure 10, providing essential context for interpreting both the stress deformation and rockfall simulation results

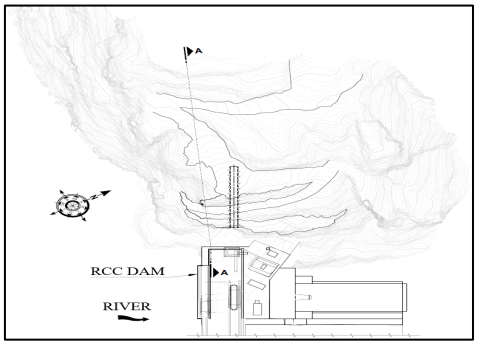

Figure 10. General layout of the left abutment slope

4.1 *Finite element (FEM) analyses*

In the context of advanced stress–strain analyses performed for the most critical rock slope section, the Jointed Rock and Jointed Rock with Mohr-Coulomb failure criterion constitutive models, as implemented in PLAXIS 2D v.2024.3, were adopted to simulate the anisotropic mechanical response of fractured rock masses. The Jointed Rock model is formulated as an anisotropic perfectly-plastic constitutive law allowing plastic failure along up to three predefined shear planes, capturing directional tensile and cohesion-friction behavior per plane (PLAXIS 2D Material Models Manual, 2024). The enhanced Iso-Jointed Rock with Mohr-Coulomb (Iso-JRMC) variant addresses the limitation of "locking" by applying an overarching Mohr-Coulomb failure envelope in principal stress space alongside explicit joint planes, enabling continuous failure progression even when discontinuity orientations deviate from predefined planes.

The PLAXIS 2D analyses were conducted following a staged construction procedure to realistically simulate the behavior of the jointed rock mass. Initially, variable lateral earth pressure coefficients (K_0) were assigned to the in-situ stresses, establishing the initial stress state for each rock and soil layer. Subsequent analyses focused on shear-triggering along discontinuities, using site-observed joint orientations and properties to guide the selection of advanced constitutive models, including Iso-JRMC and other nonlinear formulations described in the study. At each load increment, the stress tensor components acting on predefined joint planes were computed, and when the Mohr–Coulomb yield criterion was satisfied, increments of plastic shear strain ($\Delta\gamma_p$) developed in the direction of maximum shear stress. The magnitude of these strains, governed by the plastic potential and proportional to the stress excess beyond the yield surface, was superimposed onto the total strain field to capture localized slip along activated discontinuities. The Iso-JRMC formulation further incorporates a global Mohr–Coulomb envelope, allowing yielding beyond the predefined joint orientations, mitigating artificial locking, and ensuring continuous failure progression. Accumulated plastic strains were incrementally incorporated into the finite element formulation to update stress and displacement fields at each stage, enabling a robust and realistic simulation of

discontinuity-controlled deformation consistent with field observations and measured behavior.

Complementing these constitutive approaches, Schweiger et al. (2008, 2011) contributed extensively to the characterization of discontinuity behavior and anisotropic rock mass modeling, providing fundamental insights into joint orientation effects and their mechanical representation within numerical frameworks. Additionally, significant contributions from Vermeer and Brinkgreve (1994) and Alejano and Alonso (2008) have advanced the theoretical formulation and numerical implementation of jointed rock models in PLAXIS, particularly in capturing anisotropic plasticity and shear behavior along discontinuities. The collaborative research efforts of these authors have established robust methodologies for integrating complex discontinuity networks within continuum-based finite element frameworks.

These constitutive frameworks incorporate joint orientations, spacings, and strength parameters directly into the finite element mesh, enabling realistic simulation of deformation localization, stress redirection, and joint-controlled failure propagation. The sophisticated representation of rock anisotropy provided by these models significantly enhances the accuracy and resolution of slope stability predictions in structurally complex geological settings.

The incremental displacement fields associated with the Jointed Rock and Isotropic Jointed Rock with Mohr-Coulomb (Iso-JRMC) constitutive models are illustrated in Figures 11, 12 and 13, respectively, enabling a detailed comparison of deformation behavior under equivalent loading and boundary conditions. A drained condition was assumed for all constitutive models. The corresponding geomechanical input parameters employed in the finite element analyses are comprehensively summarized in Table 2.

Table 2. The constitutive parameters utilized in the simulations

Material	Parameter	Symbol	Value	Unit
Rock	Young's modulus	E	10^6	kN/m^2
	Shear modulus	G	3.9 10^5	kN/m^2
	Poisson's ratio	v	0.28	-
	Friction angle	φ	40	o
	Cohesion	c	350	kN/m^2
Discontinuities	Young's modulus	E	10^6	kN/m^2
	Shear modulus	G	3.9 10^5	kN/m^2
	Poisson's ratio	v	0.28	-
	Friction angle	φ	20	o
	Cohesion	c	80	kN/m^2
	Plane-1 dip angle	α_1	105	o
	Plane-2 dip angle	α_2	85	o
	Plane-3 dip angle	α_3	5	o

4.2 *Rock fall simulations*

Advanced two-dimensional rockfall simulations were conducted using Rocfall V8.018 to evaluate the kinematic behavior and energy distribution of potential rockfalls on the granitic slope located on the left abutment of the RCC dam. The rock mass was assumed to be a volcanic-origin granite, based on geological field surveys and discontinuity characterizations, aligning with recent methodologies proposed in the literature (Agliardi and Crosta, 2013; Giani et al., 2015).

The geometric configurations of the slope were precisely defined through high-resolution LiDAR scanning and drone-based photogrammetric surveys. These datasets were processed using Pix4D and Atlascan software to generate detailed digital surface models and three-dimensional mesh structures. This approach is in line with advanced rockfall hazard assessments where the integration of LiDAR-derived terrain data improves modeling precision (Abellan et al., 2014; Lato et al., 2015).

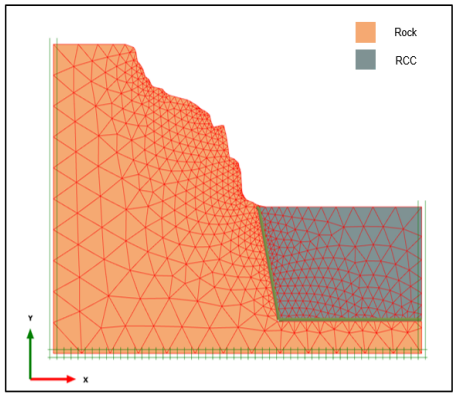

Figure 11. Finite element model

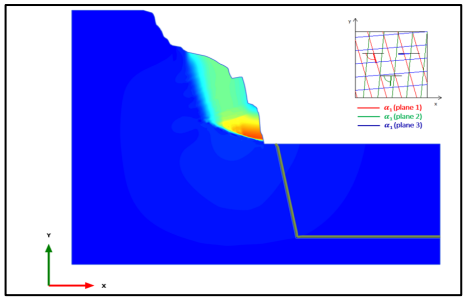
Figure 12. Incremental displacement field from the Jointed Rock model

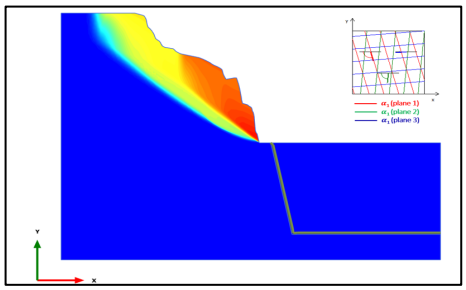
Figure 13. Incremental displacement field from the Iso-Jointed Rock with Mohr-Coulomb (Iso-JRMC) model

Critical profiles were selected from the most vulnerable sections, determined based on field-observed failures and LiDAR-based interpretations. Multiple stochastic rockfall trajectories were simulated from seeder points that represent potential detachment locations. Each simulation assessed parameters such as maximum and average kinetic energy, bounce heights, and endpoint distances, in accordance with the procedures outlined in recent rockfall analysis frameworks (Janeras et al., 2017; Tanyu et al., 2021). The rock blocks were modeled with an average size of 1 m³, which was derived from visual interpretations and LiDAR mesh evaluations of the slope, consistent with block volume estimations used in other LiDAR based rockfall studies (Tonini and Abellan, 2020).

The simulation result as presented in Figures 14, provide critical insight into expected energy magnitudes and runout

zones, which correlate well with field-mapped accumulation areas. The successful integration of numerical modeling and advanced remote sensing enhances the reliability of slope failure predictions, supporting recent research advocating for multi-source, hybrid analysis techniques in rockfall hazard assessment (Tanyu et al., 2021; Abellan et al., 2014).

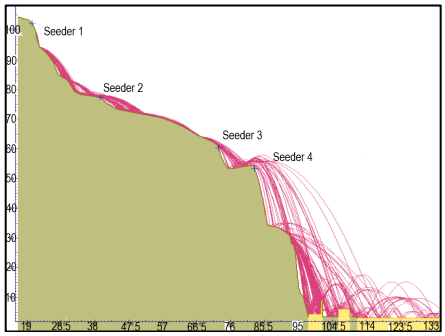

Figure 14. Rockfall simulation section

A comprehensive suite of four hundred stochastic rockfall simulations was conducted originating from four distinct seeder points to rigorously characterize the dynamic response of detached rock blocks. The analyses yielded an average kinetic energy approximating 397 kilojoules and a mean bounce height of 15.1 meters. Of particular significance, seeder points one and four were identified as zones of heightened hazard, exhibiting a quantified rockfall risk potential of seventeen point five percent. These critical initiation loci correspond to elevations of approximately 1250 meters and 1203 meters respectively. The precise spatial delineation of these high-risk sectors offers essential insights for the formulation of targeted mitigation strategies and the advancement of geotechnical risk management frameworks.

5 CONCLUSIONS

This study presents an integrated geotechnical investigation of a large scale slope instability adjacent to a roller compacted concrete (RCC) dam, utilizing high resolution LiDAR scanning, advanced numerical modeling techniques, and comprehensive geological and geotechnical characterization. The combination of these methodologies allowed for detailed mapping of the fractured granitic rock mass and accurate representation of discontinuity networks, critical for understanding complex failure mechanisms.

The deformation behavior and overall stability of the slope were assessed through detailed simulations using the Jointed Rock model and the Iso Jointed Rock with Mohr Coulomb (Iso JRMC) model. Material parameters used in the numerical analyses were derived from extensive site investigations. For the Iso JRMC model, the factor of safety against sliding was determined as F.S: 1.927, while the Jointed Rock model yielded F.S: 2.218. These results indicate a moderately critical to stable slope condition, depending on the level of structural discontinuity representation.

Moreover, the incremental displacement patterns demonstrated concentrated deformations particularly along the initial slope section and toe zone, which closely correspond to the actual failure surfaces observed on site. This high degree of correlation highlights the effectiveness and predictive capability of the applied numerical modeling framework.

Additionally, probabilistic rockfall analyses, informed by LiDAR-derived high resolution surface data, revealed that detached rock blocks predominantly followed trajectories toward the toe and mid slope zones, where calculated impact energies exceeded critical thresholds for structural damage. These findings align closely with field observations of block accumulation zones and reinforce the reliability of the integrated approach.

In conclusion, the synergy of high resolution LiDAR spatial data and physically consistent constitutive modeling has proven essential for accurately characterizing failure mechanisms in fractured rock slopes. The combined use of remote sensing and advanced numerical analyses offers a robust and transferable framework for geotechnical risk assessment and performance based slope design in dam engineering and similar infrastructure projects. Information regarding the rehabilitation of the slope through preventive and protective stabilization measures will be presented in future publications.

6 REFERENCES

Abellan, A., Martinez, J., Jaboyedoff, M., and Oppikofer, T. 2014. Terrestrial laser scanning of rock slope instabilities. Earth Surface Processes and Landforms 39(7), 878-890.

Alejano, L. R., and Alonso, E. E. 2008. Analysis of rock masses as elastoplastic jointed materials. International Journal of Rock Mechanics and Mining Sciences 45(1), 19-33.

ASTM D1196-98 (Reapproved 2018). 2018. Standard Test Method for Non-repetitive Static Plate Load Tests of Soils and Flexible Pavement Components. ASTM International, West Conshohocken, PA.

ASTM D7012-20. 2020. Standard Test Methods for Compressive Strength and Elastic Moduli of Intact Rock Core Specimens under Varying States of Stress and Temperatures. ASTM International, West Conshohocken, PA.

Hoek, E., and Brown, E. T. 1997. Practical estimates of rock mass strength. International Journal of Rock Mechanics and Mining Sciences 34(8), 1165-1186.

Hoek, E., Carranza-Torres, C., and Corkum, B. 2002. Hoek–Brown failure criterion – 2002 edition. Proceedings of the NARMS-TAC Conference 1, 267-273.

Janeras, M., López, J., and Pérez, A. 2017. Stochastic simulation of rockfall trajectories and risk assessment. Landslides 14(3), 1013-1026.

Jing, L. 2003. A review of techniques, advances and outstanding issues in numerical modelling for rock mechanics and rock engineering. International Journal of Rock Mechanics and Mining Sciences 40(3), 283-353.

Lato, M. J., Cruden, D. M., and Clague, J. J. 2015. Quantifying landslide risk using LiDAR data and GIS-based numerical rockfall simulations. Natural Hazards 76(1), 1015-1033.

Lei, X., Wang, P., and Li, X. 2020. Modelling of jointed rock masses using advanced numerical techniques: Recent developments and applications. Tunnelling and Underground Space Technology 98, 103310.

Pix4D SA. 2024. Pix4Dsurvey User Manual. Version X.X. Pix4D SA, Lausanne, Switzerland.

Schweiger, H. F., Krenn, H., and Schubert, W. 2011. Numerical modeling of anisotropic rock masses with jointed rock models. Rock Mechanics and Rock Engineering 44(3), 295-314.

Schweiger, H. F., Schubert, W., and Wellmann, F. 2008. Modeling the mechanical behavior of discontinuities in rock masses. International Journal of Rock Mechanics and Mining Sciences 45(4), 543-556.

Sheng, M., Wang, Z., and Zhang, Y. 2022. Comprehensive modelling of anisotropic rock masses using extended jointed rock models. Engineering Geology 300, 106591.

Tanyu, B. F., Yildirim, S., and Gokceoglu, C. 2021. Probabilistic rockfall hazard assessment using stochastic seeding and Monte Carlo simulation. Engineering Geology 281, 105998.

Tonini, M., and Abellan, A. 2020. Using LiDAR data for 3D rockfall source characterization and block volume estimation. Landslides 17(1), 123-138.

Vermeer, P. A., and Brinkgreve, R. B. J. 1994. A constitutive model for soils with bonded aggregates and applications to jointed rock masses. International Journal for Numerical and Analytical Methods in Geomechanics 18(8), 557-582.

PLAXIS 2D Material Models Manual. 2024. Bentley Systems.